Second-Harmonic Generation of Microwave Phonons in Quartz and Sapphire

PAUL H. CARR
Air Force Cambridge Research Laboratories, Office of Aerospace Research, L. G. Hanscom Field, Bedford, Massachusetts 01730
and
Department of Physics, Brandeis University, Waltham, Massachusetts 02154*
(Received 21 December 1967)

The phonon-phonon volume interaction due to the nonlinear elastic properties of solids has been investigated together with nonlinearities in the end-surface generation of microwave phonons. The experimental method consisted of generating a microwave-ultrasonic fundamental at one end of a rod and detecting the second harmonic at the opposite end by means of the piezoelectric effect. For Z-cut quartz and sapphire, where the phonon-phonon interaction dominates, experimental observations prove that the original flow of energy from the fundamental to the second harmonic is completely reversed after *longitudinal* waves are reflected from a stress-free surface or from a half-wavelength-thick transducer. Thus, the second harmonic in an almost lossless medium vanishes upon arrival at the generating transducer because the reflection reverses the phase angle $2\phi_1$ relative to ϕ_2, where ϕ_1 and ϕ_2 are the phase angles, respectively, of the fundamental and the second harmonic. When the thickness of the CdS transducers was made less than one-half wavelength, the smaller phase shift produced a correspondingly smaller energy reversal. For *transverse* waves in AC-cut quartz, the original increase of the second harmonic due to volume nonlinearities was unaffected by the presence of the stress-free boundary, thereby confirming that there is no phase shift for transverse waves. These phase-shift phenomena, together with the frequency and rod-length dependence of the harmonic generation, were used to separate surface from volume nonlinearities. By measuring the coupling constants of the phonon-phonon interaction at 4.2°K, the following third-order elastic coefficients (in units of 10^{11} N/m^2) were obtained: $c_{111}=-2.6\pm0.5$ for X-cut natural quartz, and -38 ± 3 for 0.01% Cr-doped a-oriented sapphire grown by the Verneuil process; $c_{333}=-14\pm4$ for Z-cut quartz, and -21 ± 1 for both undoped and 0.01% Cr-doped c-oriented sapphire.

I. INTRODUCTION

An experimental and theoretical study of the second-harmonic generation of microwave phonons in quartz and sapphire is presented in this paper. The experimental method consisted of generating a microwave-ultrasonic fundamental at one end of a rod and of detecting the second harmonic at the opposite end by the piezoelectric effect. This method was first used for studying the nonlinear elastic properties of solids at megacycle frequencies,[1,2] where the ultrasonic waves were generated and detected with quartz transducers bonded to the rod under study.

The first experiments of this type at gigacycle frequencies were done with piezoelectric X-cut quartz, where the dominant nonlinearity was found to occur in the generation process at the end surface and not in the volume of the rod.[3,4] In the present paper, the dependence of second-harmonic generation on frequency, rod length, and on phase shifts produced by reflections from the surfaces have been investigated and used as a means of separating surface and volume nonlinearities. Further insight has been gained into the mechanism by which the second harmonic is generated at the end surface of X-cut quartz. For Z-cut quartz and sapphire, where the fundamental was generated with a CdS transducer, the dominant nonlinearity was found to occur in the volume of the rod. Quantitative measurements of the second harmonic produced by this nonlinearity were used to measure the third-order elastic coefficients.

For the volume nonlinearity, we were concerned with resolving an inconsistency between different megacycle-frequency experiments. Some workers[1,5] observed that the second-harmonic longitudinal echoes increased on successive reflections; others[6] observed that the second-harmonic echoes decreased. Theoretically, the phase shift of the waves reflected from a second-harmonic-detecting resonant (one-half wavelength thick) transducer whose outer surface is stress free completely reverses the original increase of the second-harmonic amplitude, so that it vanishes at the generating transducer. Thus, no cumulative increase of the second-harmonic amplitude would be expected for a volume nonlinearity in an almost lossless medium.

The present experimental results are in good agreement with this theory, because the experimental conditions are closer to the theoretical model than those of the megacycle experiments. The plane-wave one-

* This paper is based in part on a dissertation submitted in partial fulfillment of the Ph.D. degree at Brandeis University.

[1] A. A. Gedroits and V. A. Krasil'nikov, Zh. Eksperim. i Teor. Fiz. **43**, 1592 (1962) [English transl.: Soviet Phys.—JETP **16**, 1122 (1963)].

[2] M. A. Breazeale and D. O. Thompson, J. Appl. Phys. Letters **3**, 77 (1963).

[3] P. H. Carr, Phys. Rev. Letters **13**, 332 (1964).

[4] P. H. Carr, IEEE Trans. Sonics Ultrasonics **SU-13**, 103 (1966).

[5] A. Hikata, B. B. Chick, and C. Elbaum, J. Appl. Phys. **36**, 229 (1965).

[6] M. A. Breazeale, in Proceedings of the Fifth International Congress on Acoustics, Liège, 1965, Vol. 1a, p. 18 (unpublished); M. A. Breazeale and J. Ford, J. Appl. Phys. **36**, 3486 (1965); W. B. Gauster and M. A. Breazeale, J. Acoust. Soc. Am. **41**, 860 (1967).

dimensional approximation made in the theory is valid if the ratio of the sonic wavelength to the sample diameter is much less than one. This ratio in the present experiment is at least 10^{-3}. In the megacycle experiments, it is extremely difficult to achieve this small a ratio with samples of reasonable dimensions. The phase shift that can occur inside the bond between the transducer and the sample in the megacycle experiments has been eliminated by the use of vapor deposited cadmium sulphide transducers, which have shown epitaxial growth on dielectric substrates.[7] Cadmium sulphide transducers have the additional advantage of being broadband, in that they can be used at frequencies other than those at which the transducer thickness is equal to one-half sonic wavelength. The intermediate phase shifts produced in this manner caused the observed second-harmonic echoes to undergo periodic increases and decreases. The theory has been extended to explain this dependence.

In the next section the apparatus and the general experimental method are described. In Sec. III, the theory of harmonic generation in a piezoelectric medium which includes reflection-caused phase shifts is derived. Section IV contains a discussion of the results and a comparison with the theory. Conclusions are made in Sec. V.

II. EXPERIMENTAL METHOD

Phonons at the fundamental frequency were generated by the piezoelectric effect at the end surface of a 3-mm-diam rod placed in the high-intensity electric-field region of the multiple-mode cavity shown in Fig. 1. The 5-GHz overtone resonance was lowered to approximately 4.5 GHz by means of the dielectric tuner. The acoustic fundamental was also generated in a reentrant cavity resonant in its fundamental mode at 4.5 GHz.[3,4] The generating cavity was excited by a 0.5- to 1-μsec pulse of electromagnetic energy that was passed through a low-pass filter to eliminate any harmonics above 4.5 GHz that may have been present in the pulsed-microwave source. The phonons generated in this cavity propagated to the other end of the rod, which was placed in a 9-GHz cavity. There the second-harmonic content of the acoustic wave was partially converted into microwave energy by the inverse piezoelectric effect, and the resulting signal detected by a superheterodyne receiver having a minimum sensitivity of about 10^{-12} W. The phonons reflected from the end in the 9-GHz cavity returned to the generating cavity where the fundamental acoustic energy was detected in a similar manner by a second receiver. The electromagnetic conversion efficiency (of the order of 10^{-4}) was calculated from a measurement of the ratio of the microwave signal from the first acoustic echo to the microwave power absorbed by the

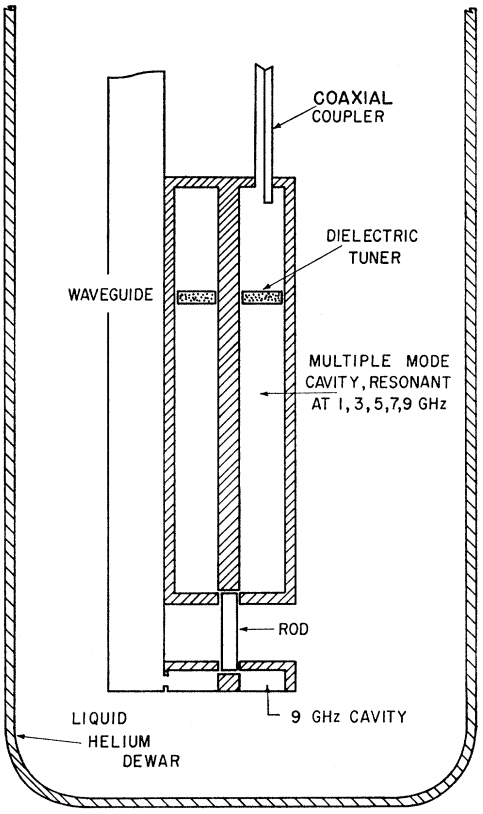

FIG. 1. Cross-sectional view of the cavity assembly used for harmonic generation and detection of microwave phonons. For second-harmonic generation, the 5-GHz resonance of the multiple-mode cavity is lowered to 4.5 GHz by means of the dielectric tuner.

4.5-GHz cavity.[8] The series of echoes generated and detected in the 4.5-GHz cavity as the wave packet underwent successive reflections from the end faces of the rod is shown in top part of Fig. 2. The second harmonic detected in the 9-GHz cavity is shown in the bottom part of Fig. 2. The beat structure superposed on the exponential decay is caused by interference effects due to the nonparallelism of the end faces.[8] This interference or beat phenomenon is consistent with the fact that the wavelength of the harmonic is one-half that of the fundamental.

The beat phenomenon complicates the measurement of the acoustic power. The detected electromagnetic power is equal to the measured electromechanical conversion efficiency times the acoustic power only when the echo envelope in Fig. 2 is extrapolated to zero distance.[8] The detected microwave power is less than this product for successive echoes, since the nonparallelism of the rod end surfaces causes the angle between them and the acoustic wavefronts to increase. However, the 9-GHz cavity assembly can be calibrated. The calibration factor depends on the frequency of the detected wave, which in this case is 9 GHz, and the

[7] J. de Klerk and E. F. Kelly, Rev. Sci. Instr. **36**, 506 (1965).

[8] P. H. Carr, J. Acoust. Soc. Am. **41**, 75 (1967).

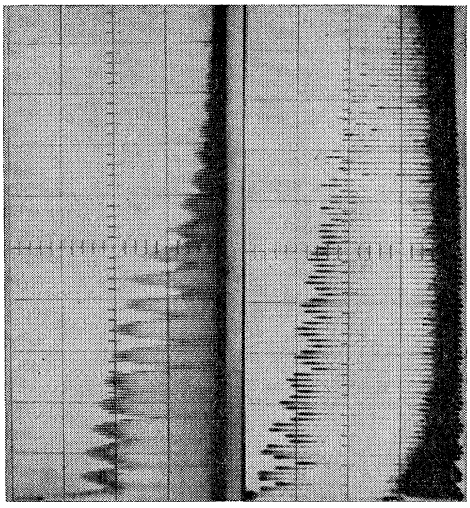

FIG. 2. Oscilloscope traces of longitudinal echoes in an X-cut quartz rod 3.0 cm long. The top trace is the 4.5-GHz fundamental, scale 200 μsec/div; the bottom trace is the second harmonic at 9.0 GHz, scale 100 μsec/div. The period of the beats scales to the frequency. No buildup of the second harmonic is observed.

number of round trips the echo has made in the rod. The calibration is made by exciting the 9-GHz cavity with a pulse of electromagnetic radiation and detecting the echoes. This procedure also allows the electromechanical efficiency of the 9-GHz cavity to be measured.

Figure 3 shows the 9-GHz second harmonic, which was harmonically generated from a 4.5-GHz fundamental, and the 9-GHz calibrating echoes, which were generated and detected in the 9-GHz cavity, plotted as a function of distance. As X-cut quartz is piezoelectric, no transducers are necessary. The power of each echo was measured by comparison with an externally generated calibrating pulse. The "0 decibels" reference on the ordinate corresponds to a second-harmonic power of 14 μW or to a second-harmonic strain amplitude $S_2(0)=(9.0\pm1)\times10^{-8}$. (The strain amplitude is equal to the amplitude of the sonic wave times its wave number k.) The acoustic power at the 4.5-GHz fundamental was 1.6 mW, corresponding to a strain amplitude $S_1=(9.5\pm1)\times10^{-7}$. The mean free paths l_1 and l_2 at the fundamental and the second harmonic, respectively, were measured by fitting the echo patterns (as on Fig. 2) to an exponential at large distances, where the amplitude modulation due to the beat phenomenon is relatively small. The 9-GHz calibrating echoes are normalized to have the same zero intercept as the second harmonic. It is apparent that the second harmonic shows no cumulative increase with respect to the calibrating echoes. This is distinctly different from the cumulative increase shown in the top part of Fig. 4 for second-harmonic generation of *transverse* waves in piezoelectric AC-cut quartz.

Second-harmonic generation with a lower 1.2-GHz fundamental has the advantage that the beat phenomenon is less pronounced. In Fig. 5 the longitudinal fundamental and the calibrating echoes decay exponentially in the a-oriented Al_2O_3 rod doped with a nominal 0.01% concentration of Cr. Thus, the end faces of the rod are parallel to a tolerance such that beats due to interference effects are not observable. When half-wavelength CdS transducers are used, the second harmonic is also observed to decay exponentially. However, when thinner transducers are used, the second harmonic is observed to undergo periodic increases and decreases, while the fundamental and calibrating echoes still decay exponentially. This dependence of the second harmonic on the transducer thickness is due to reflection produced phase shifts, which will be described in the theoretical section.

III. THEORY

A. Volume and Surface Nonlinearities

In this section the harmonic generation due to nonlinearities in the volume and at the generating surface will be described. We shall also discuss the effect that phase shifts, which are produced by reflections from the end surfaces, have on the magnitude of the second harmonic. The second harmonic of a longitudinal fundamental propagating along a pure mode axis of a piezoelectric insulator such as X-cut quartz will be obtained by solving the one-dimensional equation of motion and the nonlinear constitutive relations. The equation of motion is[9]

$$\rho\frac{\partial^2 u}{\partial t^2}=\frac{\partial}{\partial a}\left(1+\frac{\partial u}{\partial a}\right)t_1, \tag{1}$$

where ρ is the unstrained mass density, t_1 is the thermo-

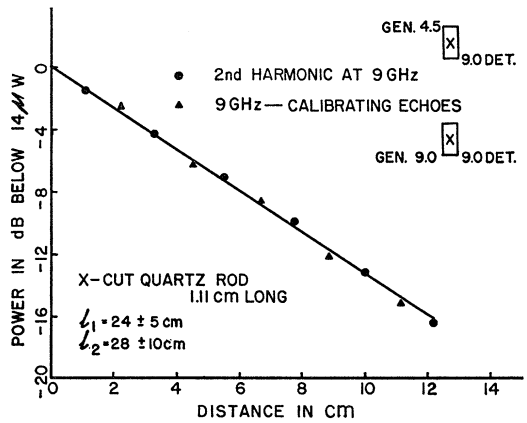

FIG. 3. Second-harmonic generation of longitudinal waves in X-cut quartz. The power of the second harmonic at 9 GHz harmonically, generated in the 4.5-GHz cavity, and the power of the 9-GHz calibrating echoes, generated and detected in the 9-GHz cavity, are plotted as a function of the distance traveled.

[9] R. N. Thurston, in *Physical Acoustics*, edited by W. P. Mason (Academic Press Inc., New York, 1964), Vol. 1, part A, p. 92.

dynamic stress,[9] and $u=x-a$. Here a is the *material* coordinate of a point that is fixed in the body, and x is the instantaneous or *spatial* coordinate.[9] The one-dimensional constitutive relations are

$$t_1=c_{11}{}^E\eta_1-e_{11}E_1+\frac{1}{2}\frac{\partial c_{11}{}^E}{\partial\eta_1}\eta_1{}^2-\frac{\partial e_{11}}{\partial\eta_1}\eta_1E_1 -\frac{1}{2}\frac{\partial e_{11}}{\partial E_1}E_1{}^2+E_1D_1-\tfrac{1}{2}\epsilon_{11}E_1{}^2, \quad (2)$$

$$D_1=e_{11}\eta_1+\epsilon_{11}E_1+\frac{1}{2}\frac{\partial e_{11}}{\partial\eta_1}\eta_1{}^2+\frac{\partial e_{11}}{\partial E_1}\eta_1E_1 +\frac{1}{2}\frac{\partial\epsilon_{11}}{\partial E_1}E^2+\cdots. \quad (3)$$

Here η_1 is the strain, E_1 is the electric field, D_1 is the electric displacement, $c_{11}{}^E$ is the elastic coefficient at constant electric field, ϵ_{11} is the dielectric constant at constant strain, and e_{11} is the piezoelectric coefficient at constant strain. The "sub 1" refers, for the case of quartz, to the X axis, which is along the axis of the rod.

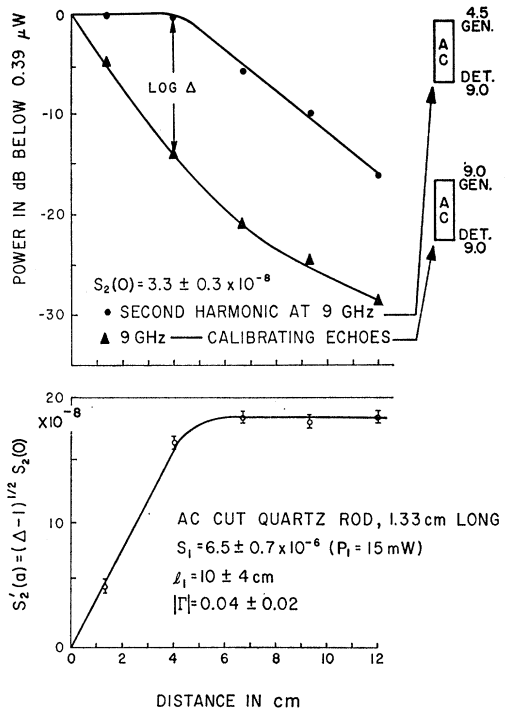

FIG. 4. Second-harmonic generation of transverse waves in *AC*-cut quartz. Top: The measured acoustic power of the second harmonic and calibrating echoes are plotted as a function of distance traveled. The increase of the second harmonic with respect to the calibrating echoes shows that the second harmonic was generated in the volume of the rod. Bottom: Plot of the quantity $S_2'(a)$, which has the dimensions of strain amplitude and is defined in the text, as a function of distance. The solid curve represents the theoretically predicted dependence of $S_2'(a)$ which is fitted to the experimental points for a value of $\Gamma=0.04\pm0.02$.

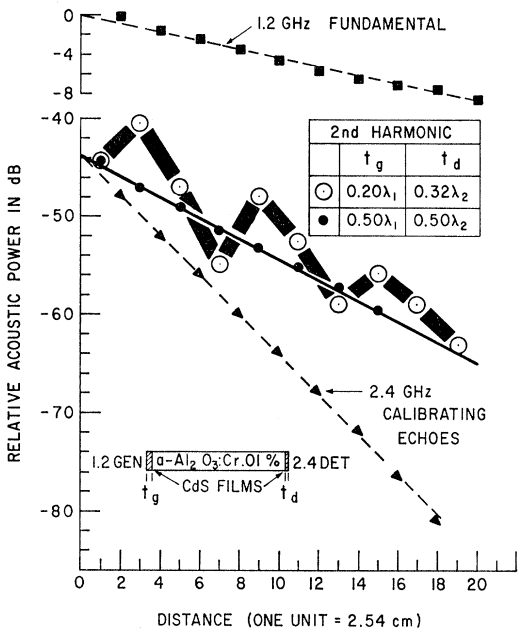

FIG. 5. Second-harmonic generation of longitudinal waves in an *a*-oriented, 2.54-cm-long ruby rod. The relative acoustic power is plotted as a function of distance. The second harmonic decays exponentially or oscillates depending on the thickness of the CdS transducers. λ_1 and λ_2 are the sonic wavelengths of the fundamental and second harmonic, respectively.

These constitutive relations can be derived from the thermodynamic potential $\tilde{F}$ of Landau and Lifshitz[10] (or equivalently, from the potential G_2 of Mason).[11] The following identity[12] is useful in relating $\partial e_{11}/\partial E_1$ to the photoelastic constant p_{11}:

$$\frac{\partial e_{11}}{\partial E_1}=-\frac{\partial\epsilon_{11}}{\partial\eta_1}=\epsilon_{11}{}^2\frac{p_{11}}{\epsilon_0}. \quad (4)$$

$\partial\epsilon_{11}/\partial E_1$ can be related to the electro-optic constant r_{11}:

$$\frac{\partial\epsilon_{11}}{\partial E_1}=-\epsilon_{11}{}^2\frac{r_{11}}{\epsilon_0}. \quad (5)$$

The coefficient $\partial c_{11}/\partial\eta_1$ is equal to the thermodynamic definition[13] of the third-order elastic coefficient c_{111}.

By first solving Eq. (3) for E_1 (the nonlinear terms are second-order quantities), we find that Eqs. (1)

[10] L. D. Landau and E. M. Lifshitz, *Electrodynamics of Continuous Media* (Addison-Wesley Publishing Co., Inc., Reading, Mass., 1960), pp. 70–79.

[11] W. P. Mason, *Physical Acoustics and the Properties of Solids* (D. Van Nostrand Co., Inc., Princeton, N. J., 1958), p. 373.

[12] A. J. Slobodnik, Jr., Air Force Cambridge Research Laboratory Physical Science Research Paper, No. 319, 1967 (unpublished).

[13] K. Brugger, Phys. Rev. **133**, A1611 (1964).

and (2) become

$$\frac{\partial^2 u}{\partial a^2}-\frac{1}{v_{11}^2}\frac{\partial^2 u}{\partial t^2}=+\frac{\partial}{\partial a}\frac{e_{11}}{c_{11}^D\epsilon_{11}}D_1$$
$$-\frac{\partial}{\partial a}\left[\epsilon_{11}+\frac{\partial\epsilon_{11}}{\partial\eta_1}+\frac{e_{11}}{\epsilon_{11}}\frac{\partial\epsilon_{11}}{\partial E_1}\right]\frac{D_1^2}{2\epsilon_{11}c_{11}^D}$$
$$+\frac{\partial}{\partial a}\left(\frac{\partial u}{\partial a}\right)\frac{D_1}{\epsilon_{11}E_{2f}}-\frac{1}{2}\frac{\partial}{\partial a}\left(3+\frac{c_{111}^D}{c_{11}^D}\right)\left(\frac{\partial u}{\partial a}\right)^2, \quad (6)$$

where

$$c_{11}^D=c_{11}^E+e_{11}^2/\epsilon_{11}, \quad (7a)$$

$$v_{11}^2=c_{11}^D/\rho, \quad (7b)$$

$$c_{111}^D=c_{111}^E-e_{11}^2/\epsilon_{11}+3\frac{e_{11}}{\epsilon_{11}}\left(\frac{\partial e_{11}}{\partial\eta_1}\right)$$
$$+3\left(\frac{e_{11}}{\epsilon_{11}}\right)^2\left(\frac{\partial\epsilon_{11}}{\partial\eta_1}\right)+\left(\frac{e_{11}}{\epsilon_{11}}\right)^3\left(\frac{\partial\epsilon_{11}}{\partial E_1}\right), \quad (7c)$$

and

$$c_{11}^D E_{2f}^{-1}=\frac{\partial e_{11}}{\partial\eta_1}+2\frac{e_{11}}{\epsilon_{11}}\left(\frac{\partial\epsilon_{11}}{\partial\eta_1}\right)+\left(\frac{e_{11}}{\epsilon_{11}}\right)^2\left(\frac{\partial\epsilon_{11}}{\partial E_1}\right). \quad (7d)$$

Here we have made use of Eq. (4) and the definition $\eta_1=(\partial u/\partial a)+\frac{1}{2}(\partial u/\partial a)^2$. Since the electric displacement field D_1 produced by the external electromagnetic source vanishes outside the reentrant cavity (see Fig. 1), the nonlinear terms proportional to D_1 can generate a second harmonic only within the small portion of the rod inside the cavity; the term proportional to $(\partial u/\partial a)^2$ can produce harmonics throughout the entire volume of the rod.

We shall solve Eq. (6) by assuming a solution:

$$u=u_1\sin(k_1a-\omega_1t)+u_2, \quad (8a)$$

$$\partial u/\partial a=S_1\cos(k_1a-\omega_1t)+(\partial u_2/\partial a), \quad (8b)$$

where u_1 is the solution of the linear equation and u_2 is the trial solution for the second harmonic. The linear equation has been solved.[14] The strain amplitude

$$S_1=k_1u_1=e_{11}D_1/c_{11}^D\epsilon_{11}. \quad (9)$$

The fundamental is generated at the end surface of the rod by the discontinuity of the piezoelectric constant.[14] Generation of the fundamental in the volume is not possible since the wavelength of the microwave-frequency radiation is the order of a centimeter, while the wavelength of the phonons is the order of a micron.

The second-harmonic strain amplitude, obtained by substituting Eq. (8) into Eq. (6) and by using the perturbation approximation $|u_2|\ll|u_1|$, is

$$k_2u_2=S_2(0)\cos 2(k_1a-\omega_1t)$$
$$+S_2(a)\cos[2(k_1a-\omega_1t)-\tfrac{1}{2}\pi], \quad (10)$$

where

$$S_2(0)=\frac{D_1^2}{4c_{11}^D\epsilon_{11}^2}\left[\epsilon_{11}\left(\frac{\epsilon_{11}}{\epsilon_0}-1\right)\right.$$
$$\left.-\frac{\partial\epsilon_{11}}{\partial\eta_1}-\frac{e_{11}}{\epsilon_{11}}\left(\frac{\partial\epsilon_{11}}{\partial E_1}\right)+\frac{2e_{11}}{c_{11}^D}\left(\frac{\partial e_{11}}{\partial\eta_1}\right)\right] \quad (11)$$

represents the second-harmonic strain amplitude generated at the end surface, $a=0$, and

$$S_2(a)=\tfrac{1}{4}\Gamma_1S_1^2k_1a \quad (12)$$

represents the second harmonic generated in the volume of the rod. The coupling constant for the phonon-phonon interaction.

$$\Gamma_1=3+c_{111}^D/c_{11}^D. \quad (13)$$

Here we have made use of the weak-coupling approximation, namely, that the electromechanical coupling factor $K^2=e_{11}^2/c_{11}^D\epsilon_{11}$ is much less than unity. This approximation is well satisfied for quartz and cadmium sulphide, where K^2 is 0.009 and 0.024, respectively. The second-harmonic contribution from the spatial dependence of D_1^2 was found negligibly small for the same reason that the volume contribution for the linear case was also negligible.[14]

The term $S_2(0)$, which is proportional to D_1^2, can cause harmonic generation in a nonpiezoelectric medium (i.e., $e_{11}=0$). Here the generation is due to the radiation pressure or Maxwell-Faraday stress, which arises from the discontinuity at the end surface of the dielectric constant $(\epsilon_{11}/\epsilon-1)$, and to the discontinuity of the electrostrictive coefficient $\partial\epsilon_{11}/\partial\eta_1$. Quantitative measurements of harmonic generation in nonpiezoelectric Z-cut quartz and sapphire have been made,[4] and the contribution from the Maxwell-Faraday term was found to be much larger than that from the electrostrictive term.[15] For the piezoelectric case, there are additional contributions arising from the discontinuity of the electro-optic coefficient, $\partial\epsilon_{11}/\partial E_1$, and from the strain dependence of the piezoelectric coefficient, $\partial e_{11}/\partial\eta_1$. By eliminating D_1^2 from Eq. (11) with the use of Eq. (9), we find for longitudinal surface generation in a piezoelectric medium that

$$S_2(0)=\tfrac{1}{4}S_1^2K^{-2}\left[\epsilon_{11}\left(\frac{\epsilon_{11}}{\epsilon_0}-1\right)\right.$$
$$\left.-\frac{\partial\epsilon_{11}}{\partial\eta_1}-\frac{e_{11}}{\epsilon_{11}}\left(\frac{\partial\epsilon_{11}}{\partial E_1}\right)+\frac{2e_{11}}{c_{11}^D}\left(\frac{\partial e_{11}}{\partial\eta_1}\right)\right]. \quad (14)$$

[14] E. H. Jacobsen, J. Acoust. Soc. Am. 32, 949 (1960).

[15] This experiment is of additional interest since it is believed to be the first observation of the temporal variation of the electromagnetic radiation stress. The now classic experiments [E. Whittaker, *Aether and Electricity* (Harper and Row, New York, 1960), Vol. I, p. 275] for measuring the radiation pressure of light detected the static component of the pressure.

The term $S_2(a)$ for the volume nonlinearity given by Eq. (12) differs from the surface nonlinearity $S_2(0)$ by its frequency and volume dependence. $S_2(a)$ is proportional to the phonon frequency (since $k_1=2\pi f_1/v$) and to the distance a the phonons have traveled. $S_2(0)$ is independent of f_1 and a. From a quantum-mechanical viewpoint, the surface nonlinearity corresponds to the destruction of two photons and to the creation of one phonon in a process where wave vectors are not conserved; while the volume nonlinearity corresponds to the descruction of two phonons and to the creation of one phonon in a process where wave vectors are conserved.[16] The different frequency and length dependence of the surface and volume nonlinearities gives a means of separating them.

Equation (12) for the volume harmonic generation may be used in a nonpiezoelectric medium where the fundamental S_1 is excited with a piezoelectric CdS transducer. Equation (14) for the nonlinear surface generation of longitudinal waves in a piezoelectric medium may not be used when a piezoelectric CdS transducer is deposited onto a nonpiezoelectric rod, because the additional boundary between the CdS and the rod will introduce an additional multiplicative factor. This factor will not concern us at present, since for those materials in which CdS transducers were used, the nonlinearity in the volume was always much greater than in the transducer.

B. Phase Shifts

The phase shifts caused by the reflection from the end surfaces of the rod give an additional means of separating surface and volume nonlinearities. The nonlinear interaction producing $S_2(0)$ is "turned off" as the phonon wave packet propagates away from the generating surface. Thus, if the surface nonlinearity were much larger than the volume nonlinearity, $S_2(0)$ would essentially remain constant as the wave packet propagated in a lossless acoustic medium. On the other hand, the nonlinear volume interaction producing $S_2(a)$ is "on" all the time during propagation. As will be seen, the original energy flow from the fundamental to the second harmonic is completely reversed after longitudinal waves are reflected from a stress-free surface, and the second-harmonic echo vanishes when it arrives at the generating surface. This behavior is produced by the phase shift of the fundamental with respect to the second harmonic.

The phase shift $\Delta\phi$ of a longitudinal wave reflected from a transducer, whose outer surface is stress free, is

$$e^{i\Delta\phi}=\frac{iZ_t\tan k_t t-Z_r}{iZ_t\tan k_t t+Z_r}, \tag{15}$$

where Z_t and Z_r are the acoustic impedances, respectively, of the transducer and the rod, k_t is the wave vector in the transducer, and t is the transducer thickness. This formula follows from transmission line theory when the transducer is treated as a transmission line terminated by a short circuit. (The acoustic stress is represented by its voltage analog.[17]) The outer surface of the transducer is stress free, as the acoustic impedance of the liquid helium in which it is immersed is much less than that of the transducer. Acoustic losses in the transducer have been neglected, as the experimental transducers were only of the order of a half-wavelength thick. Equation (15) is valid for the steady-state condition, which is reached in a time 1/100 of the experimental pulse width. In the derivation of this equation, use was again made of the weak-coupling approximation. It is interesting to note that when the transducer is one-half wavelength thick, the phase shift is the same as that from a stress-free surface, i.e., $\Delta\phi=180°$.

We shall now find how the reflection-caused phase shift affects the amplitude of the second harmonic. The relative phase angle between the fundamental having a phase angle ϕ_1 and the second harmonic having a phase angle ϕ_2 is defined as $2\phi_1-\phi_2=\theta$. It is apparent in Eq. (10), which represents the perturbation solution for the nonlinear volume term of Eq. (6), that θ has a constant value of 90°. Equation (10) is valid for an infinite medium, but when boundaries are present, a more general solution must be found. This is done in Appendix A, where a more general trial solution [than that of Eq. (8)] yields explicit relations between the relative phase angle θ and the strain amplitude of the second harmonic

$$S_2^2(a)=(\tfrac{1}{4}\Gamma_1 S_1^2 k_1 a)^2+S_{20}^2+\tfrac{1}{2}S_{20}\Gamma_1 k_1 a\sin\theta_0, \tag{16}$$

and

$$S_{20}\cos\theta_0=S_2(a)\cos\theta(a). \tag{17}$$

Here S_{20} and θ_0 refer to initial values. In deriving these formulas, which are valid for the lossless case, the perturbation assumption, $S_2\ll S_1$, was made. This also implies that S_1 is a constant. In addition it has been assumed that $S_2(a=L)$, where L is the length of the rod, is much larger than $S_2(0)$. From Eqs. (10) and (17) it follows that $\theta=90°$ just before reflection from the end surface at $a=L$. Immediately after reflection, $\theta_0=90°+\Delta\theta$, where $\Delta\theta$ is the phase shift due to the reflection, and $S_{20}=S_2(L)=\frac{1}{4}\Gamma S_1^2 k_1 L$. Thus, when the waves arrive back at the generating surface

$$S_2(2L)=\tfrac{1}{4}\sqrt{2}\Gamma_1 S_1^2 k_1 L(1+\cos\Delta\theta)^{1/2} \tag{18}$$

and

$$\theta(2L)=\cos^{-1}[S_2(L)/S_2(2L)]. \tag{19}$$

The value of $S_2(3L)$, $\theta(3L)$, etc., can be computed in an analogous manner by the successive use of Eqs. (16) and (17).

[16] P. H. Carr, Ph.D. dissertation, Brandeis University, 1966 (unpublished).

[17] J. C. Sethares, Air Force Cambridge Research Laboratory Physical Science Research Paper No. 262(I), 1966 (unpublished).

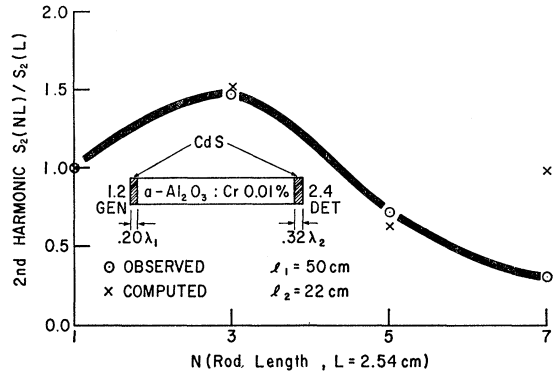

FIG. 6. Second-harmonic strain amplitude (normalized with respect to the first echo) plotted as a function of the number of times the wave packet has traversed the 2.54-cm-long rod shown in Fig. 5. The observed points agree with the points which were computed from the theory, which is valid as long as the length of travel NL is much less than the phonon mean free path.

Equation (18) shows the importance that the phase shift has on the second harmonic. For a longitudinal wave reflected from a stress-free surface, the phase shift of both the fundamental and the second harmonic is 180°, so $\Delta\theta=180°$.[18] Thus the second harmonic vanishes at the generating surface $a=2L$. For a transverse wave whose particle motion is parallel to the end surface (as in AC-cut quartz) the fundamental and the second harmonic are reflected with no change in phase.[18] Thus the second harmonic at the end surface $a=2L$ is twice the value at the surface $a=L$. For a longitudinal wave reflected from a transducer which is one-half wavelength thick (at the second-harmonic frequency), the second harmonic undergoes a phase shift of 180°, as predicted by Eq. (15), and the fundamental has no phase shift. Thus $\Delta\theta=-180°$, and the second harmonic vanishes at the surface $a=2L$, as it did for the case of a single stress-free surface.

The theoretical treatment so far has been for a lossless elastic medium. Equation (12) may be generalized for a lossy medium having mean free paths l_1 and l_2 at the fundamental and second-harmonic frequencies, respectively, by replacing a with a_{eff}, where

$$a_{\text{eff}}=\frac{e^{-a/l_2}-e^{-2a/l_1}}{2/l_1-1/l_2}. \tag{20}$$

a_{eff} is equal to a for $a\ll l_1,l_2$ and has a maximum value for $a=0.69l_1$ (for $l_1=l_2$).[4,16] In the present experiment, the criterion that a given sample be lossless is that the sample length L be much less than the mean free paths l_1 and l_2. In those cases where the second harmonic would have vanished at the generating transducer in the lossless case, the second harmonic in the lossy case will be slightly greater than zero. This is because the energy lost from the second harmonic due to the irreversible scattering process, which is responsible for its attenuation, is not available to be transferred back to the fundamental.

TABLE I. Frequency and length dependence of the second-harmonic strain amplitude $S_2(L)$.

Sample	Length (cm)	~1.2-GHz fundamental $S_2/S_1^2(10^4)$	~1.2-GHz fundamental $(4.5/1.2)\times S_2/S_1^2(10^4)$	~4.5-GHz fundamental $S_2/S_1^2(10^4)$
c-Al_2O_3	1.91	0.39±0.06	1.5±0.2	1.7 ±0.4
a-Al_2O_3 0.01% Cr^{+3}	2.54	2.1 ±0.3	8.1±1	6.0 ±1.5
X-SiO_2	1.0[a]	0.81±0.1	3.2±0.5	2.0 ±0.5
X-SiO_2	3.1[a]	0.77±0.1	3.1±0.5	1.7 ±0.4
X-SiO_2	1.1	0.85±0.1	3.1±0.5	4.9 ±1
X-SiO_2	1.3	0.87±0.1	3.2±0.5	4.4 ±1
AC-SiO_2	1.3	0.16±0.02		0.13±0.03[b]

[a] These two samples were cut from the same 4.1-cm-long, X-cut quartz rod.
[b] Taken from zero intercept.

IV. DISCUSSION OF RESULTS

A. Sapphire

The distance or volume dependence of the second harmonic observed in Fig. 5 for a-oriented sapphire is in agreement with the theoretical predictions for a *volume* linearity. For the case where the CdS transducers are one-half wavelength thick, the second harmonic decays exponentially with a slope intermediate between that of the fundamental and the 2.4-GHz calibrating echoes. This is in agreement with the theoretical prediction that the second harmonic vanishes at the generating transducer. If the second harmonic had been predominantly generated by nonlinearities in the generating transducer, it would have decayed with the slope of the 2.4-GHz calibrating echoes.

Additional confirmation for a volume effect is given by the periodic increases and decreases observed in Fig. 5 with transducers of thickness $0.20\lambda_1$ and $0.32\lambda_2$, where λ_1 and λ_2 are the sonic wavelengths, respectively, of the fundamental and the second harmonic. A comparison between the observed second-harmonic strain amplitude S_2 and that computed with Eqs. (16) and (17) is shown in Fig. 6. The first computed second-harmonic echo is normalized equal to $S_2(L)$, the strain amplitude of the first second-harmonic echo observed in the rod of length L. The phase shifts at the generating and detecting transducers, $\Delta\theta_g=-74.5°$ and $\Delta\theta_d=-76°$, were computed with Eq. (15) from the measured transducer thicknesses and the sonic velocity, 4.76×10^5 cm/sec. This value gave a better fit to the observed echoes than did the bulk value, which is 10% lower. De Klerk has also observed that the sonic velocity of CdS films is, depending on the deposition rate, from 5 to 10% higher than the bulk value.[19] Good agreement in Fig. 6 between the observed and computed values is

[18] Reference 11, pp. 22–27.

[19] J. de Klerk (private communication).

seen for the second and third echoes. The fourth echo is observed to be smaller than its computed value. This deviation might have been expected since the length of travel, $NL=18$ cm, is of the same magnitude as the mean free path. The theoretical computation is valid only when the length of travel is much less than the mean free path.

For the c-oriented sapphire rod shown in Fig. 7, an attempt was made to fabricate CdS transducers of thickness such that the second harmonic would monotonically increase. This would be expected from the curve computed with $t_g=0.258\lambda_1$, $t_d=0.416\lambda_2$, $\Delta\theta_g=164°$, and $\Delta\theta_d=-102°$. The first two observed echoes are in reasonable agreement with the computed points. However, if a computation is made using film thicknesses which differ from the above by the 2.5% thickness-measurement accuracy, $\Delta\theta_g=149°$, $\Delta\theta_d=-109°$, and a curve which has a maximum is obtained. The last two observed echoes are closest to this curve. The rapid variation of $\Delta\theta$ with thickness is due to the fact that $\tan k_t t$ in Eq. (15) is in a rapidly varying region. The sensitivity of the phase shift to $k_t t$ might be of potential use in measuring this product. Our present purpose, however, is to show that the observed second harmonic is dominantly produced by nonlinearities in the volume of the rod. Thus, the agreement between theory and experiment is adequate.

Additional confirmation for a dominant volume nonlinearity is shown in Table I. The numbers in column 4 were obtained by multiplying S_2/S_1^2, which was obtained from the 1.2-GHz fundamental, by the 4.5/1.2 frequency ratio of the two different fundamentals. It is evident by comparing columns 4 and 5 that the second-harmonic strain amplitude for sapphire is proportional to frequency. The nonlinear surface-generated term $S_2(0)$ is, by contrast, independent of frequency and must therefore, be much smaller than the volume term. The frequency and volume dependence verify that the dominant nonlinearity occurs in the volume of the rod.

The measured values of the phonon-phonon coupling constant Γ, which were computed from Table I with the use of Eq. (12), are listed in Table II. The Al_2O_3 samples were all grown by the Verneuil process. The 0.01% Cr-doped samples were obtained from the Adolf Meller Company and the undoped c-oriented specimen was grown at the Air Force Cambridge Research Laboratories. It is apparent that the magnitude of Γ is, within experimental uncertainty, independent of the doping. Since it is not known whether Γ has a plus or minus sign, the sign of the third-order elastic coefficients computed from Eq. (13) was chosen to agree with that measured by a static method,[20] which consisted of measuring the change in velocity of a low-amplitude ultrasonic wave when the sample was subjected to uniaxial and hydrostatic stress.

[20] J. H. Gieske, Ph.D. dissertation, Pennsylvania State University, 1968 (unpublished).

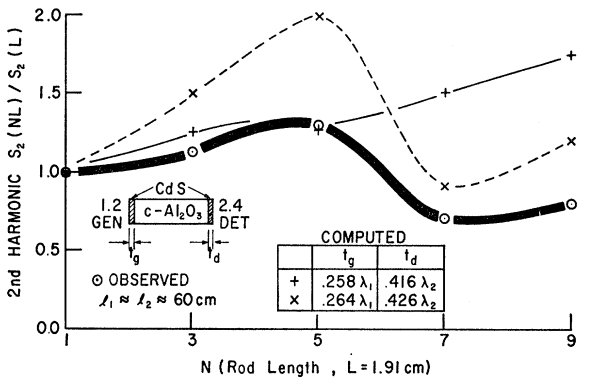

FIG. 7. Second-harmonic strain amplitude (normalized with respect to the first echo) plotted as a function of the number of times the wave packet has traversed a 1.91-cm-long, c-oriented, sapphire rod. The two different sets of transducer thicknesses differ by the 2.5% measurement uncertainty.

B. *AC*-Cut Quartz

In this section we shall discuss the results for transverse waves in AC-cut quartz, where it will be seen that both surface and volume terms are of comparable magnitude. In the top part of Fig. 4, the second-harmonic power at 9 GHz generated from a 4.5-GHz fundamental is plotted as a function of distance. The calibrating echoes generated and detected at 9 GHz are plotted in an identical manner, their $a=0$ intercept being normalized to equal that of the second harmonic. The zero intercept of the second harmonic measures the nonlinearity in the generating process, while the increase of the second harmonic above the calibrating echoes Δ is a measure of the volume nonlinearity. The details of the method of separating the surface from the volume nonlinearities and of eliminating destructive interference effects are described in Appendix B. The volume

TABLE II. Measurement of the phonon-phonon coupling constant Γ and the third-order elastic coefficients.

		Experiment[a]		Literature[b]
Sample	Γ_1	c_{11} (10^{11} N/m^2)	c_{111} (10^{11} N/m^2)	c_{111} (10^{11} N/m^2)
X-SiO_2	$\lesssim 0.5$	0.87±0.06	−2.6±0.5	−2.1±0.07[c]
a-Al_2O_3 0.01% Cr	4.8±0.7	4.9 ±0.1	−38±3	−39.1[d]
	Γ_3	c_{33}	c_{333}	c_{333}
Z-SiO_2	8±3	1.2±0.1	−14±4	−8.15±0.18[c] −10.2[e]
c-Al_2O_3 0.01% Cr	1.1±0.2	5.1±0.1	−20±1	28.8 or 30.9[d]
c-Al_2O_3 (undoped)	1.3±0.2	5.1±1	−22±1	28.8 or 30.9[d]
AC-SiO_2[f]	0.01 to 0.1			

[a] The present experiment was performed at helium temperature.
[b] Measured at room temperature.
[c] Reference 22.
[d] Reference 20.
[e] Reference 21.
[f] Measured for transverse waves. Longitudinal waves were used for the other samples.

nonlinearity obtained from Eq. (B4) is

$$S_2'(a)=[\Delta(a)-1]^{1/2}S_2(0)=\tfrac{1}{4}\Gamma_1 S_1^2 k_1 a, \quad a\ll l \quad (21a)$$

$$S_2'(a)=\tfrac{1}{4}\Gamma_1 S_1^2 k_1 l, \quad a\gg l \quad (21b)$$

where $l_1=l_2=l$.

In the bottom part of Fig. 4, the quantity $S_2'(a)$ is plotted as a function of the distance and is fitted to the experimental points with $\Gamma=0.04\pm0.02$ and $l_1=l_2=7+3$ cm. This value of the mean free path is equal within experimental error to the measured value of 10 ± 4 cm, which was obtained by fitting the fundamental frequency echoes to an exponential in the region where interference effects were the smallest. In the region of a less than the stabilization distance (a mean free path of 7 ± 3 cm corresponds to a stabilization distance of 5 ± 2 cm),[4] the linear increase of $S_2(a)$ with a predicted by Eq. (21a) is followed. The straight line passes through the origin as it must from the extrapolations in the top part of Fig. 4. The value of Γ computed from Eq. (21a) is 0.04 ± 0.02, the uncertainty being due to the experimental error. The value of Γ, computed from Eq. (21b) in the region where a is much greater than the stabilization distance, is equal within experimental error to that computed from Eq. (21a). The agreement between the predicted variation of $S_2'(a)$ and that actually observed confirms that there is no phase shift for transverse waves at a stress-free surface. Thus, in effect, the boundary does not influence the second-harmonic generation of transverse waves whose particle motion is parallel to the surface.

The frequency dependence of the second-harmonic generation was investigated with the use of a 1.2-GHz fundamental. Here, it was found that the second-harmonic echoes did not increase with respect to the calibrating echoes. Thus, the surface nonlinearity is much larger than the volume nonlinearity. The latter would be expected to be smaller at 1.2 GHz than at 4.5 GHz owing to the frequency dependence of the interaction [Eq. (12)]. It can be seen in Table I that $S_2(0)$ is independent of frequency to within the experimental uncertainty. This agrees with the surface nonlinearities described by Eq. (14). This equation, which is valid for longitudinal waves, may be applied to transverse waves in AC-cut quartz by replacing the longitudinal components of the photoelastic, electro-optic, and piezo-strain coefficients by the relevant transverse components and by setting the Maxwell-Faraday stress term which is proportional to $(\epsilon_{11}/\epsilon_0-1)$ equal to zero. The transverse Maxwell-Faraday stress is proportional to the transverse component of the electric field, which is very small in the experimental configuration.

The Γ values measured for three different AC-cut rods ranged from 0.01 to 0.1. This variation may mean that impurities or dislocations are affecting the volume harmonic generation. It is apparent in Table II that the phonon-phonon coupling constant for transverse waves in AC-cut quartz is much smaller than for longitudinal waves in sapphire and quartz.

C. Z-Cut Quartz

The dominant nonlinearity for longitudinal waves propagating along the nonpiezoelectric Z axis of quartz was found to occur in the volume of the rod by detecting the second harmonic both at the same end of the rod at which the fundamental was generated and at the opposite end. The fundamental was generated by a $4.67\ \lambda_1/2$-thick CdS transducer at the end of the rod placed in the multiple-mode cavity shown in Fig. 1. The second harmonic was detected by a $3.01\ \lambda_1/2$-thick transducer on the opposite end, which was placed in the 9.4-GHz reentrant cavity. When the acoustic wave packet arrived back at the generating cavity, the second harmonic was again detected, as the frequency of the multiple-mode cavity had been adjusted so that it was resonant at both 4.7 and 9.4 GHz. This was accomplished by locating the dielectric tuner at a position near the coupling-loop-end of the cavity where the electric field for the ~9-GHz mode was a minimum while the electric field for the ~5-GHz mode was a maximum. Thus, the ~5-GHz mode was lowered to one-half the frequency of the ~9-GHz mode, which was unaffected by the presence of the dielectric.

The second-harmonic acoustic power, detected at the same end of the rod at which the fundamental was generated, was found to be two orders of magnitude smaller than the second-harmonic power detected at the opposite end. When the $3.01\ \lambda_1/2$ second-harmonic-detecting transducer was removed, so that both the fundamental and the second harmonic were reflected from the stress-free surface, the observed second harmonic detected with the $4.67\ \lambda_1/2$-thick transducer was three orders of magnitude smaller than that detected by the $3.01\ \lambda_1/2$ transducer when it was present. This behavior is consistent with the theoretical prediction that the second harmonic produced by a volume nonlinearity in a lossless acoustic medium vanishes when it returns to the generating surface. A similar behavior has recently been observed in an experiment in which the second harmonic was detected by an optical method.[21] The small residual second harmonic detected at the fundamental-generating transducer could be due to nonlinearities in this transducer or to the fact that the acoustic medium is not completely lossless. The sample length was about $\frac{1}{5}$ of the estimated acoustic mean free path. The values of the phonon-phonon coupling constant Γ and the third-order elastic coefficient c_{333} are listed in Table II. The sign of c_{333} was chosen to agree with that measured by a static method.[22]

---

[21] R. B. Thompson, C. D. W. Wilkinson, and B. A. Richardson, Stanford University Microwave Laboratory Report No. 1561, 1967 (unpublished).

[22] R. N. Thurston, H. J. McSkimin, and P. Andreatch, Jr., J. Appl. Phys. **37**, 267 (1966).

D. *X*-Cut Quartz

The dominant nonlinearity for longitudinal waves propagating along the piezoelectric X axis of quartz was found to occur at the end surface of the rod. In Table I it can be seen that the second harmonic S_2/S_1^2 for two X-cut rods 1 and 3.1 cm long, which were cut from the same 4.1-cm long rod, is independent of the sample length. Since the second harmonic for the volume nonlinearity is proportional to the sample length [Eq. (12)] while that for the surface generation nonlinearity is independent of the sample length [Eq. (14)], the latter dominates over the former. In this experiment the 1.2-GHz fundamental and 2.4-GHz second harmonic were detected at opposite ends of the rod. Thus, the above conclusion is based on the assumption that the elastic properties of the original 4.1-cm sample were homogeneous. This assumption was validated by detecting the second harmonic both at the same end of the rod at which the fundamental was generated and at the opposite end in a manner identical to that used for Z-cut quartz (except that CdS transducers were not needed). In contrast to the results obtained for Z-cut quartz, the second harmonic detected at each end was the same, a result consistent with a dominant surface nonlinearity. The small volume nonlinearity for X-cut quartz implies that the acoustic attenuation caused by the phonon-phonon interaction should be very small.[23]

The upper limit of Γ listed in Table II was calculated with the use of Eq. (12) by assuming that the contribution from the volume nonlinearity was equal to the observed surface nonlinearity in the 3.1-cm-long rod. Since Γ is the difference between two relatively large numbers, a fairly accurate value for $c_{111}{}^D$ is obtained. The difference between $c_{111}{}^D$ and $c_{111}{}^E$ indicated in Eq. (7c) is less than 6%. This can be seen from a numerical calculation using the tabulated values of the linear coefficients[24] and the following values of the nonlinear coefficients (which are consistent with microwave rectification[25] and radiation pressure generation[4] experiments): $\partial e_{11}/\partial\eta_1 \approx 0.4$ C m^{-2}, $\partial\epsilon_{11}/\partial\eta_1 \approx -3\times10^{-11}$ C/V m, and $\partial\epsilon_{11}/\partial E_1 \approx -10^{-22}$ C V^{-2}. Thurston *et al.*[22] have also observed that the difference between the third-order elastic coefficients at constant electric field and at constant electric displacement was less than their experimental uncertainty.

The dominant physical mechanism for the surface nonlinearity in X-cut quartz is much larger than that given in Eq. (14). The contribution of the Maxwell-Faraday stress term in this equation gives a value $S_2(0)/S_1^2=88$ and the contribution from the nonlinear coefficients is an order of magnitude less than this. The observed value in Table I is $S_2(0)/S_1^2=10^4$. The fact that $S_2(0)/S_1^2$ is nearly proportional to the phonon frequency [Eq. (14) is frequently independent] and is independent of sample length could indicate that the second harmonic is being generated by a volume nonlinearity in the vicinity of the generating surface. It is possible that the effective value of the phonon-phonon coupling constant Γ could be much larger near this surface due to defects introduced by optical polishing.[8] Another possibility might be a noncollinear phonon-phonon interaction between a longitudinal phonon and a transverse phonon[26] generated by fringing fields in the reentrant cavity. It is nevertheless evident that the nonlinear surface generation mechanism in X-cut quartz is not due to the Maxwell-Faraday stress or the nonlinear coefficients in the constitutive relations.

V. CONCLUSIONS

For a volume nonlinearity, experimental observations prove that the original energy flow from the fundamental to the second harmonic is completely reversed after *longitudinal* waves are reflected from a stress-free surface or from a half-wavelength-thick transducer whose outer surface is stress free. Thus, the second harmonic in an essentially lossless elastic medium vanishes upon arrival at the generating transducer. This behavior was explained by the reflection-produced phase shift of the fundamental with respect to the second harmonic. The smaller phase shift produced by a CdS transducer whose thickness was less than a half wavelength caused a less complete reversal of the energy flow, so that more round trips or echoes were needed to produce a minimum in the observed second harmonic. For *transverse* waves in AC-cut quartz, there was no phase shift and consequently no reversal of the energy flow. Thus, energy reversal occurs for longitudinal but not for transverse waves.

The coupling constant for the phonon-phonon volume interaction has been measured and related to the third-order elastic coefficients. As can be seen in Table II, these coefficients, which were measured at gigacycle frequencies and at helium temperature, agree for X-cut quartz and a-oriented ruby with static measurements[20,22] made at room temperature. The agreement for Z-cut quartz and c-oriented sapphire and ruby is not so good. One possible reason for this discrepancy might be differing contribution from dislocations[5] and crystal imperfections. This possibility is evidenced by the fact that Gieske[20] obtained the value $c_{333}=28.8\times10^{11}$ N/m^2 from uniaxial measurements alone and the value 30.9×10^{11} N/m^2 from both hydrostatic and uniaxial measurements. Some caution should also be made in comparing third-order elastic coefficients measured at room temperature with those measured at helium temperature. Temperature variations ranging from 10 to 20% have been computed for crystals of the alkali-

[23] M. G. Blair and E. H. Jacobsen, Phys. Letters **23**, 647 (1966).
[24] R. Bechmann, A. D. Ballato, and T. J. Lukaszek, Proc. IEEE **50**, 1812 (1960).
[25] P. H. Carr and A. J. Slobodnik, Jr., J. Appl. Phys. **38**, 5153 (1967).
[26] F. R. Rollins, Jr., L. H. Taylor, and P. H. Todd, Jr., Phys. Rev. **136**, A597 (1964).

halide type.[27,28] In any event, there appears to be no appreciable dispersion in the third-order elastic coefficients from static to gigacycle frequencies.

Nonlinearities in the generation process were observed for piezoelectric X- and AC-cut quartz. The nonlinear end-surface generation for transverse waves in AC-cut quartz was found to be independent of the phonon frequency. Thus, the generation could be due to the electric field and strain dependence of the dielectric coefficient and the strain dependence of the piezoelectric coefficient. The larger second harmonic of longitudinal waves in X-cut quartz was observed to be proportional to the phonon frequency. This suggests that the second harmonic was produced by a volume interaction within the end of the rod inserted in the high electric-field region of the reentrant cavity.

ACKNOWLEDGMENTS

I wish to thank Professor S. Berko for helpful discussions during the early stages of this research. I also wish to thank Dr. J. de Klerk for the fabrication of the CdS transducers and assistance in measuring their thickness, Dr. M. A. Breazeale for helpful discussions about the boundary conditions, and Professor G. R. Barsch for information about the static values of the third-order elastic coefficients of sapphire prior to their publication. The AFCRL Verneuil-grown sapphire was kindly supplied by the Crystal Growth Branch of the Solid State Sciences Laboratory. Technical assistance during the course of the experiments was provided by T/Sgt J. H. Silva.

APPENDIX A

In this Appendix, a solution which explicitly shows the effect of the phase shift on the volume nonlinearity of Eq. (6) will be found. The approach is similar to that used by Armstrong *et al.*[29] for the interactions of light waves in a nonlinear dielectric. When the assumed solution

$$2\frac{\partial u(a)}{\partial a}=[S_{1c}e^{i(k_1a-\omega_1t)}+S_{1c}{}^{*}e^{-i(k_1a-\omega_1t)}]+[S_{2c}e^{i(k_2a-\omega_2t)}+\text{c.c.}], \quad \text{(A1)}$$

where $S_{1c}=S_1e^{i\phi 1}$, is inserted in Eq. (6) and when use is made of the fact that $\partial^2S/\partial a^2\ll k(\partial S/\partial a)\ll k^2S$, the following coupled equations are obtained:

$$\frac{\partial S_1}{\partial a}=-\tfrac{1}{4}\Gamma k_1S_1S_2\sin\theta, \quad \text{(A2)}$$

$$\frac{\partial S_2}{\partial a}=\tfrac{1}{4}\Gamma S_1{}^2\sin\theta, \quad \text{(A3)}$$

$$\frac{\partial\theta}{\partial a}=(2k_1-k_2)-\frac{\cos\theta}{\sin\theta}\frac{\partial}{\partial a}\ln S_1{}^2S_2, \quad \text{(A4)}$$

where $\theta=2\phi_1-\phi_2$. These equations are to be solved subject to the constraint that the total elastic energy W is constant.

$$W=\tfrac{1}{2}\rho v^3A[S_1{}^2+S_2{}^2]=\tfrac{1}{2}\rho v^3AS_1{}^2(0), \quad \text{(A5)}$$

where A is the area of the rod. In the last step we have assumed that the second harmonic at the end surface $S_2(0)$ is much less than the fundamental $S_1(0)$.

The effect of the dispersion term in Eq. (A4), $(2k_1-k_2)$, is very small. A calculation[16] using the dispersion relation of a linear chain showed that dispersion effects for a 4.5-GHz fundamental are negligible up to distances of $\sim$100 cm. Since this is generally much less than the experimental mean free path, the dispersion factor $2k_1-k_2$ will be neglected.

Further simplification can be obtained with the following:

$$u=(\rho v^3A/2W)^{1/2}S_1=S_1/S_1(0), \quad \text{(A6)}$$

$$v=(\rho v^3A/2W)^{1/2}S_2=S_2/S_1(0), \quad \text{(A7)}$$

$$\zeta=(2W/\rho v^3A)^{1/2}\tfrac{1}{4}k_1a\Gamma=\tfrac{1}{4}\Gamma S_1(0)k_1a. \quad \text{(A8)}$$

Thus, Eqs. (A2) to (A5) become

$$\frac{\partial u}{\partial\zeta}=-uv\sin\theta, \quad \text{(A9)}$$

$$\frac{\partial v}{\partial\zeta}=u^2\sin\theta, \quad \text{(A10)}$$

$$\frac{\partial\theta}{\partial\zeta}=\frac{\cos\theta}{\sin\theta}\frac{\partial}{\partial\zeta}\ln u^2v, \quad \text{(A11)}$$

$$u^2+v^2=1. \quad \text{(A12)}$$

These equations are identical with Eq. (5.5) of Armstrong *et al.*[29] for the harmonic generation of light in a nonlinear dielectric.

Equation (A11) can be integrated to give a constant of integration:

$$G=u^2v\cos\theta. \quad \text{(A13)}$$

The solution for the case $G\neq 0$, $v\ll 1$, and $u=1$ can be obtained from Eq. (5.14a) of Armstrong *et al.*[29]

$$v^2=\zeta^2+v_0{}^2+2\zeta v_0\sin\theta_0, \quad \text{(A14)}$$

where v_0 and θ_0 are initial values. Equations (16) and (17) in the text follow directly from Eqs. (A14) and (A13), respectively.

APPENDIX B

In this Appendix the method of separating surface from volume nonlinearities and of eliminating destructive interference due to end-surface nonparallelism will

[27] A. A. Nran'yan, Fiz. Tverd. Tela **5**, 177 (1963) [English transl.: Soviet Phys.—Solid State **5**, 129 (1963)].
[28] P. B. Ghate, Phys. Rev. **139**, A1666 (1965).
[29] J. A. Armstrong, N. Bloembergen, J. Decuing, and P. S. Pershan, Phys. Rev. **127**, 1918 (1962).

be described. The method is illustrated in Fig. 4, where the second-harmonic power at 9 GHz generated from a 4.5-GHz fundamental is plotted as a function of distance. The calibrating echoes generated and detected at 9 GHz are plotted in an identical manner, their $a=0$ intercept being normalized to equal that of the second harmonic. The zero intercept of the second harmonic measures the nonlinearity in the generating process, while the increase of the second harmonic above the calibrating echoes Δ is a measure of the volume nonlinearity.

The detected second-harmonic microwave power $P_{2m}(a)$ is given by

$$P_{2m}(a)=IF_2(a)[P_2(a)+P_2(0)e^{-2a/l_2}], \quad \text{(B1)}$$

where I is the insertion loss or electromechanical conversion efficiency, $F_2(a)$ is the destructive interference factor, which has the property of being equal to one at $a=0$,[8] and $P_2(a)$ and $P_2(0)$ are the acoustic powers corresponding to the volume and surface terms $S_2(a)$ and $S_2(0)$, respectively. The microwave calibrating pulse $P_c(a)$ which is surface generated and detected at 9 GHz, is given by

$$P_c(a)=IF_2(a)P_2(0)e^{-2a/l_2}, \quad \text{(B2)}$$

where $F_2(a)$ is the same as in Eq. (B2), since the frequency is the same. For the present purposes the absolute power level of $P_c(a)$ is arbitrary, and we have chosen $P_c(a)$ in Eq. (B2) to be equal to $P_2(0)$ at $a=0$, as is shown graphically in the top part of Fig. 4. $F_2(a)$ is now eliminated by dividing Eq. (B1) by Eq. (B2):

$$[\Delta(a)-1]P_2(0)=P_2(a)e^{2a/l_2}, \quad \text{(B3)}$$

where $\Delta(a)=P_{2m}(a)/P_c(a)$.

It is convenient for a graphical plot of the experimental results to take the square root of Eq. (B3) and to define a new quantity $S_2'(a)$:

$$S_2'(a)=(\Delta(a)-1)^{1/2}S_2(0)$$

$$=\tfrac{1}{4}\Gamma S_1^2 k_1\left[\frac{1-e^{-2a/l_1+a/l_2}}{2l_1^{-1}-l_2^{-1}}\right]. \quad \text{(B4)}$$

Here we have used Eqs. (12) and (20). Equation (B4) thus gives a relation for the volume nonlinearity which is independent of the end-surface nonparallelism. Equations (21a) and (21b) in the text come from Eq. (B4).

PHYSICAL REVIEW VOLUME 169, NUMBER 3 15 MAY 1968

F Center in Ionic Crystals: Semicontinuum Polaron Models

HERBERT S. BENNETT
National Bureau of Standards, Washington, D. C. 20234
(Received 1 November 1967; revised manuscript received 18 December 1967)

The states of the F center are considered on the basis of models which treat the movement of the nearest neighbors to the F center and the F electron in a self-consistent manner. The lattice is described in terms of a classical ionic-crystal theory, and the F electron is treated according to the semicontinuum polaron theory. The absorption energy, the emission energy, the lifetime of the first excited state, the thermal activation energies, and the Huang-Rhys factor are evaluated for two models (Hartree and quasiadiabatic) which differ in the evaluation of the optical polarization. It is shown that the Hartree semicontinuum polaron model agrees best with the experimental results for NaCl, KCl, CaF_2, SrF_2, and BaF_2. In addition, these models show that among the above quantities the thermal activation energies and the lifetime of the first excited state are most sensitive to the physical content of a given model.

I. INTRODUCTION

THE F center in ionic crystals consists of an electron localized about a vacant negative-ion site. Even though the F center is one of the simplest defects which can occur in ionic crystals, calculations of its optical properties have been a challenge to theoreticians ever since Tibbs first undertook such calculations for the alkali halides.[1] Most calculations of the F-center electronic structure consider the ground state and the low-lying excited states in a rigid lattice, are valid only for optical-absorptive transitions, and view the lattice either as a continuum or as an array of point ions.[2–4] However, electronic polarization (distortion of the closed shells of the ions) and ionic polarization (displacement of the ions) are present and are factors which influence the energy levels of the F electron. Only a few authors have attempted to include these polarizations

[1] S. R. Tibbs, Trans. Faraday Soc. **35**, 147 (1934).

[2] S. I. Pekar, Usp. Fiz. Nauk **50**, 197 (1953).

[3] B. S. Gourary and F. J. Adrian, Phys. Rev. **105**, 1180 (1057).

[4] J. K. Kubler and R. J. Friauf, Phys. Rev. **140**, A1742 (1965).

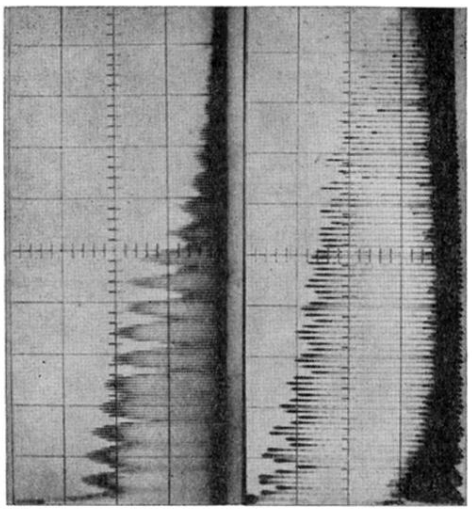

FIG. 2. Oscilloscope traces of longitudinal echoes in an X-cut quartz rod 3.0 cm long. The top trace is the 4.5-GHz fundamental, scale 200 μsec/div; the bottom trace is the second harmonic at 9.0 GHz, scale 100 μsec/div. The period of the beats scales to the frequency. No buildup of the second harmonic is observed.